Hindawi Publishing Corporation
EURASIP Journal on Wireless Communications and Networking
Volume 2009, Article ID 306876, 11 pages
doi:10.1155/2009/306876

Research Article

Dynamic Model of Signal Fading due to Swaying Vegetation

Michael Cheffena[1] and Torbjörn Ekman[2]

[1] *University Graduate Center (UNIK), P.O. Box 70, 2027 Kjeller, Norway*
[2] *Department of Electronics and Telecommunications, Norwegian University of Science and Technology, 7491 Trondheim, Norway*

Correspondence should be addressed to Michael Cheffena, cheffena@yahoo.com

Received 31 July 2008; Revised 1 December 2008; Accepted 18 February 2009

Recommended by Michael A. Jensen

In this contribution, we use fading measurements at 2.45, 5.25, 29, and 60 GHz, and wind speed data, to study the dynamic effects of vegetation on propagating radiowaves. A new simulation model for generating signal fading due to a swaying tree has been developed by utilizing a multiple mass-spring system to represent a tree and a turbulent wind model. The model is validated in terms of the cumulative distribution function (CDF), autocorrelation function (ACF), level crossing rate (LCR), and average fade duration (AFD) using measurements. The agreements found between the measured and simulated first- and second-order statistics of the received signals through vegetation are satisfactory. In addition, Ricean K-factors for different wind speeds are estimated from measurements. Generally, the new model has similar dynamical and statistical characteristics as those observed in measurements and can thus be used for synthesizing signal fading due to a swaying tree. The synthesized fading can be used for simulating different capacity enhancing techniques such as adaptive coding and modulation and other fade mitigation techniques.

1. Introduction

In a given environment, radiowaves are subjected to different propagation degradations. Among them, vegetation movement due to wind can both attenuate and cause a fading effect to the propagating signal. Operators cannot guarantee a clear line-of-sight (LOS) to wireless customers as vegetation in the surrounding area may grow or expand over the years and obstruct the path. Fade mitigation techniques (FMTs) such as adaptive coding and modulation can be used to counteract the signal fading caused by swaying vegetation. For example, during windy conditions (high signal fading), power efficient modulation schemes such as BPSK and QPSK (which are less sensitive to propagation impairments compared to high-order modulation schemes) can be used to increase the link availability, while spectral efficient modulation schemes such as 16 QAM and 64 QAM can be applied during calm wind conditions (less signal fading) [1]. An extra coding information can also be added to the channel so that errors can be detected and corrected by the receiver. FMTs need to track the channel variations and adjust their parameters (modulation order, coding rate, etc.) to the current channel conditions. In order to design, optimize, and test FMT, data collected from propagation measurements are needed. However, such data may not be available at the preferred frequency, wind speed conditions, and so forth. Alternatively, time series generated from simulation models can be used. In this case, the simulated time series need to have similar dynamical and statistical characteristics as those obtained from measurements [1].

The signal attenuation depends on a range of factors such as tree type, whether trees are in leaf or without leaf, whether trees are dry or wet, frequency, and path length through foliage [2, 3]. For frequencies above 20 GHz, leaves and needles have large dimensions compared to the wavelength, and can significantly affect the propagation conditions. The ITU-R P.833 [4] provides a model for predicting the mean signal attenuation though vegetation. The temporal variations of the relative phase of multipath components due to movement of the tree result in fading of the received signal as reported in, for example, [5–10]. The severity of the fading depends on the rate of phase changes which further depends on the movement of the tree components. Therefore, for accurate prediction of the channel characteristics, the motion of trees under the influence of wind should be taken into account. This requires the knowledge of wind dynamics and

the complex response of a tree to induced wind force. In our previous work, a heuristic approach was used to model the dynamic effects of vegetation [10]. In this paper, we develop a theoretical model based on the motion of trees under the influence of wind, and is validated in terms of first- and second-order statistics using available measurements.

The paper begins in Section 2 by giving a brief description of the measurement setup for measuring signal fading after propagating through vegetation and for measuring meteorological data (wind speed and precipitation). Section 3 discusses the wind speed dynamics. The motion of trees and their dynamic effects on propagating radiowaves as well as the validation of the proposed simulation model are dealt with in Section 4. Finally, conclusions are presented in Section 5.

2. Measurement Setup

To characterize the influence of vegetation on radiowaves, measurements were performed in [7] for a broad range of frequencies, including 2.45, 5.25, 29, and 60 GHz, in various foliage and weather conditions. A sampling rate of 500 Hz was used to collect the radio frequency (RF) signals using a spectrum analyzer, multimeter, and a computer with General Purpose Interface Bus (GPIB) interface. In order to understand the behavior of radiowaves propagating through vegetation under different weather conditions, meteorological measurements including wind speed and precipitation were also performed in [7]. The wind speed was recorded every 5 seconds, and the precipitation data every 10 seconds.

The measurements were taken at two different locations, referred to as Site 1 and Site 2. The trees at Site 1 were deciduous trees, and were considered both when the trees were in full leaf and when they were without leaf. Site 2 was populated by several coniferous trees which made a wall of trees. Table 1 gives a general site information. A detailed description of the measurements can be found in [7]. An example of received signal at 29 GHz after propagating through dry leaved deciduous trees (Site 1) is shown in Figure 1, and the corresponding measured wind speed is shown in Figure 2. These figures indicate a strong dependency of the signal variation transmitted through vegetation on the wind speed. For a closer look, Figures 3 and 4 show examples of typical measured signals during low (1 to 3 m/s) and high (≥4.5 m/s) wind speed conditions for leaved dry deciduous trees (Site 1) at 29 GHz. As expected, we can observe that the signal variation increases with increasing wind speed. Accurate modeling of the channel is needed when designing mitigation techniques for the fast and deep signal variations are like the ones shown in Figures 1 and 4. In order to do this, a good knowledge of wind dynamics and trees motions due to wind is required.

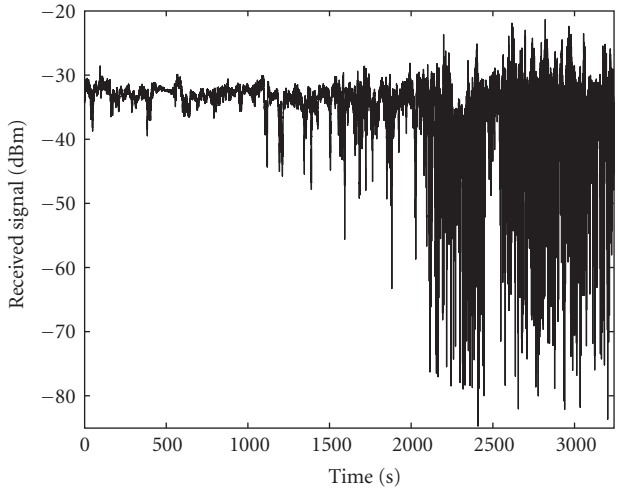

Figure 1: Measured signal fading after propagating through dry leaved deciduous trees (Site 1) at 29 GHz. A sampling rate of 500 Hz was used to collect the signal.

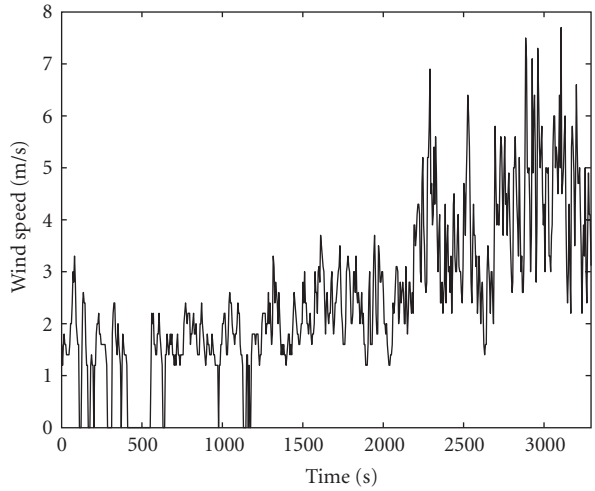

Figure 2: Measured wind speed for the corresponding signal fading shown in Figure 1. The wind speed was measured every 5 seconds.

3. Wind Dynamics

Trees sway mostly due to wind. Understanding the dynamic characteristics of wind is therefore essential when describing the complex response of a tree to induced wind force and their dynamic effects on propagating radiowaves. The turbulent wind speed power spectrum can be represented by a Von Karman power spectrum [11], and it can be simulated by passing white noise through a shaping filter with transfer function given by [12, 13]

$$H_F(s) = \frac{K_F}{(1 + sT_F)^{5/6}}, \tag{1}$$

where K_F and T_F are the gain and time constant of the shaping filter, respectively. A close approximation of the 5/6-order filter in (1) by a rational transfer function is given by [12]

$$H_F(s) = K_F \frac{(g_1 T_F s + 1)}{(T_F s + 1)(g_2 T_F s + 1)}, \tag{2}$$

Table 1: Site description [7].

Site	Path length	Foliage depth	Description
Site 1	63.9 m	14.3 m	3 foliated maple trees
		7.6 m	1 foliated flowering crab tree
Site 2	110 m	25 m	Several spruce and one pine tree creating a wall

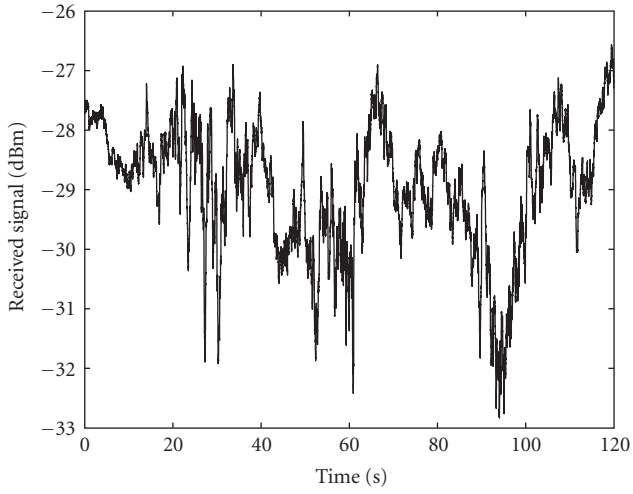

Figure 3: Typical measured signal at 29 GHz for leaved dry deciduous trees (Site 1) during low-wind speed conditions (1 to 3 m/s). A sampling rate of 500 Hz was used to collect the signal.

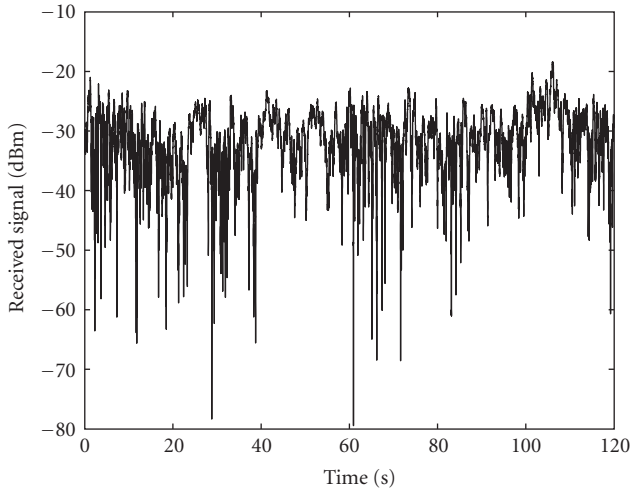

Figure 4: Typical measured signal at 29 GHz for leaved dry deciduous trees (Site 1) during high-wind speed conditions (≥4.5 m/s). A sampling rate of 500 Hz was used to collect the signal.

where $g_1 = 0.4$ and $g_2 = 0.25$. T_f and K_F are defined as

$$T_F = \frac{L_r}{w_m}, \tag{3}$$

$$K_F \approx \sqrt{\frac{2\pi}{B(1/2, 1/3)} \frac{T_F}{T_s}}, \tag{4}$$

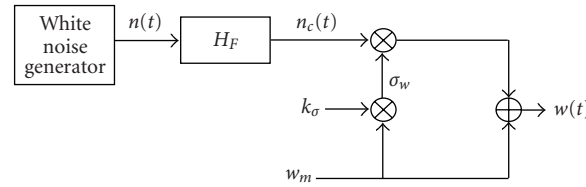

Figure 5: Model for simulating wind speed. $n(t)$ is a white Gaussian noise with zero mean and unite variance, H_F is the low-pass filter defined in (2), $n_c(t)$ is a colored noise, k_σ is a model parameter (see Table 2), w_m is the mean wind speed, $\sigma_w = w_m k_\sigma$, and $w(t)$ is the resulting wind speed.

Table 2: k_σ values for different terrain types at 10 meter height [14].

Type	Coastal	Lakes	Open	Built-up areas	City centers
k_σ	0.123	0.145	0.189	0.285	0.434

where w_m is the mean wind speed and L_r is the turbulence length scale that corresponds to the site roughness. The turbulence length can be calculated from the height, h, above the ground, expressed as $L_r = 6.5h$ [14]. T_s is the sampling period and B designates the beta function, and is given by

$$B(u, y) = \int_0^1 z^{u-1}(1-z)^{y-1} dz. \tag{5}$$

Figure 5 shows the model for simulating wind speed. In the model, a white Gaussian noise $n(t)$ (where t is the time) with zero mean and unite variance is transformed into colored noise $n_c(t)$ by smoothing it with the filter given in (2). The static gain K_F defined in (4) ensures that the resulting colored noise $n_c(t)$ has a unit variance. The wind speed $w(t)$ is then obtained by multiplying $n_c(t)$ by the standard deviation of the turbulent wind σ_w and adding the mean wind speed w_m. k_σ is a constant which depends on the type of the terrain [14]; see Table 2. This wind model is used in Section 4.1 to describe the displacement of tree due to induced wind force.

4. The Dynamic Effects of Vegetation on Radiowaves

4.1. The Motion of Trees. A tree is a complex structure consisting of a trunk, branches, subbranches, and leaves. The tree responds in a complex way to induced wind forces, with each branch swaying and dynamically interacting with other branches and the trunk. During windy conditions, first-order branches sway over the swaying trunk, and second-order branches sway over the swaying first-order branches. Generally, smaller branches sway over swaying

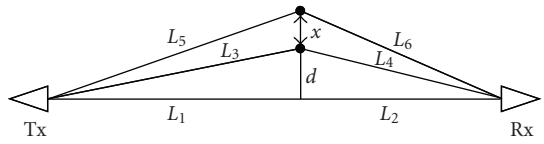

Figure 6: Path length difference. L_1+L_2 is the path length of the LOS component, $L_3 + L_4$ is the path length of the multipath component at rest, $L_5 + L_6$ is the path length of the multipath component when displaced, x is the displacement, d is the distance from the LOS path to the position of a tree component. Tx and Rx are the transmitting and receiving antennas.

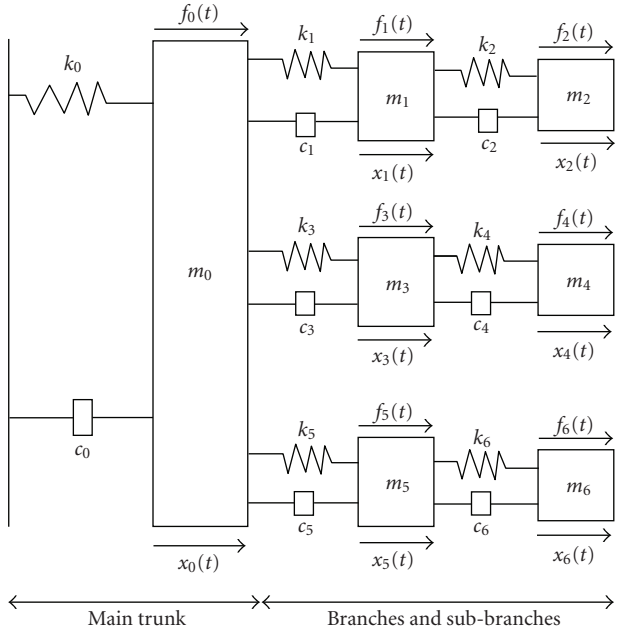

Figure 7: Dynamic representation of a tree. m_i, k_i, c_i, $f_i(t)$, and $x_i(t)$ are the mass, spring constant, damping factor, time varying wind force, and time varying displacement of tree component i, respectively.

larger branches, and leaves vibrate over swaying smaller branches. The overall effect minimizes the dynamic sway of the tree by creating a broad range of frequencies and prevents the tree from failure [15]. Radiowaves scattered from these swaying tree components have a time varying phase changes due to periodic changes of the path length which results in fading of the received signal. Figure 6 illustrates the path length difference due to displacement of a tree component from rest, and is given by (see Appendix A)

$$\Delta L \approx x\frac{d(L_1 + L_2)}{L_1 L_2}, \tag{6}$$

where $L_1 + L_2$ is the path length of the LOS component. L_1 is the distance from the transmitter to a point parallel to a position of a tree component, d is the distance from the point to the position of a tree component, L_2 is the distance from the point parallel to a position of a tree component to the receiver, and x is the displacement.

A dynamic structure model of tree was reported in [15], and is extended here to include dynamic wind force and mathematical description of the motion of each tree component; see Figure 7. In the model, tree components (the trunk, branches, and subbranches) are attached with each other using springs which resulted in a multiple mass-spring system. This tree model is further used in Section 4.2 to model the signal fading due to swaying vegetation. For simplicity, we use a tree model with a trunk and just three branches and three subbranches, as seen in Figure 7. This simple model is sufficient to recreate the rich dynamic behavior of the fading from a real tree, as is demonstrated in the simulations in Section 4.2. Using Newton's second law and the Hooke's law, the equations of motion (displacement) for the tree components in Figure 7 can be formulated using second-order differential equations:

$$\begin{aligned}
m_0\ddot{x}_0(t) &= -\dot{x}_0(t)(c_0 + c_1 + c_3 + c_5) + \dot{x}_1(t)c_1 + \dot{x}_3(t)c_3 \\
&\quad + \dot{x}_5(t)c_5 - x_0(t)(k_0 + k_1 + k_3 + k_5) + x_1(t)k_1 \\
&\quad + x_3(t)k_3 + x_5(t)k_5 + f_0(t), \\
m_1\ddot{x}_1(t) &= -\dot{x}_1(t)(c_1 + c_2) + \dot{x}_2(t)c_2 + \dot{x}_0(t)c_1 \\
&\quad - x_1(t)(k_1 + k_2) + x_2(t)k_2 + x_0(t)k_1 + f_1(t), \\
m_2\ddot{x}_2(t) &= c_2(\dot{x}_1(t) - \dot{x}_2(t)) + k_2(x_1(t) - x_2(t)) + f_2(t), \\
m_3\ddot{x}_3(t) &= -\dot{x}_3(t)(c_3 + c_4) + \dot{x}_4(t)c_4 + \dot{x}_0(t)c_3 \\
&\quad - x_3(t)(k_3 + k_4) + x_4(t)k_4 + x_0(t)k_3 + f_3(t), \\
m_4\ddot{x}_4(t) &= c_4(\dot{x}_3(t) - \dot{x}_4(t)) + k_4(x_3(t) - x_4(t)) + f_4(t), \\
m_5\ddot{x}_5(t) &= -\dot{x}_5(t)(c_5 + c_6) + \dot{x}_6(t)c_6 + \dot{x}_0(t)c_5 \\
&\quad - x_5(t)(k_5 + k_6) + x_6(t)k_6 + x_0(t)k_5 + f_5(t), \\
m_6\ddot{x}_6(t) &= c_6(\dot{x}_5(t) - \dot{x}_6(t)) + k_6(x_5(t) - x_6(t)) + f_6(t),
\end{aligned} \tag{7}$$

where m_i, k_i, and c_i are the mass, spring constant, and damping factor of tree component i, respectively. The spring constant k_i describes the stiffness of the wood material. While the damping factor c_i describes the energy dissipation due to swaying tree component (aerodynamic damping) and dissipation from internal factors such as root/soil movement and internal wood energy dissipation [15]. $\ddot{x}_i(t)$, $\dot{x}_i(t)$, and $x_i(t)$ are the acceleration, velocity, and position (displacement) of tree component i, respectively. $f_i(t)$ is the time varying induced wind force on tree component i, and is given by [16]

$$f_i(t) = \frac{C_d \rho w_i(t)^2 A_i}{2}, \tag{8}$$

where C_d is the drag coefficient, ρ is the air density, A_i is the projected surface area of the tree component, and $w_i(t)$ is the wind speed (can be simulated using the model shown in Figure 5).

The time varying displacement, $x_i(t)$, of each tree component can then be obtained by solving (7) using state-space modeling:

$$\dot{\mathbf{y}} = \mathbf{A}\mathbf{y} + \mathbf{B}\mathbf{u}, \tag{9}$$

$$\mathbf{x} = \mathbf{C}\mathbf{y} + \mathbf{D}\mathbf{u}, \tag{10}$$

where $\mathbf{y} = \left[x_0(t) \ \cdots \ x_6(t) \ \dot{x}_0(t) \ \cdots \ \dot{x}_6(t)\right]^T$ is the state vector, $\mathbf{u} = \left[f_0(t) \ \cdots \ f_6(t)\right]^T$ is the input vector, and $\mathbf{x} = \left[x_0(t) \ \cdots \ x_6(t)\right]^T$ is the output vector. The matrices **A**, **B**, **C**, and **D** are obtained from (7); see Appendix B. Note that (9) and (10) are for continuous time and can be converted to discrete time using, for example, bilinear transformation.

4.2. Signal Fading due to Swaying Tree. Former studies on the measurements used here suggested that the signal envelope can be represented using the extreme value or lognormal distribution [7]. However, our study shows that the Nakagami-Rice distribution can well represent the measured signal envelop through vegetation. The Chi-Square test has been performed to verify the fitness of Nakagami-Rice and measured signal distribution. For all frequencies, the hypothesis was accepted for 5% significance level. Furthermore, the majority of reported measurement results suggest Nakagami-Rice envelop distribution [8, 17–19]. Therefore, Nakagami-Rice envelop distribution is assumed in the developed simulation model, with the K-factor given by

$$K = \frac{P_d}{P_f}, \tag{11}$$

where P_d and P_f are the power in the direct and diffuse components, respectively. From our measurements, we estimated the Ricean K-factors under different wind conditions using the moment-method reported in [20]; see Figure 8. The reduction of the K-factor suggests that the contribution of the diffuse component increases with increasing wind speed. We can also observe that the K-factor decreases with increasing frequency (due to smaller wavelength).

The time series for the received power is obtained as $|h(t)^2|$, where $h(t)$ is the complex impulse response due to the multipath in the vegetation. For a Ricean distributed signal envelope, the impulse response $h(t)$ can be expressed as the sum of the direct and diffuse signal components as shown in

$$h(t) = \underbrace{a_d \exp(j\theta)}_{\text{Direct}} + \underbrace{\sum_{i=1}^{N=7} a_f \exp\left[j\left(\theta_i - \frac{2\pi}{\lambda}\Delta L_i(t)\right)\right]}_{\text{diffuse}}, \tag{12}$$

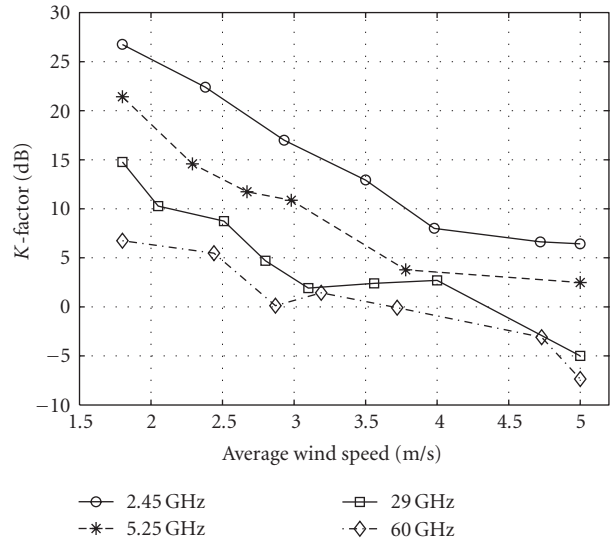

Figure 8: Ricean K-factors as function of average wind speed estimated from measurements at 2.45, 5.25, 29, and 60 GHz after propagating through dry leaved deciduous trees (Site 1).

where the first term in (12) is the contribution of the direct signal component. $a_d = \sqrt{P_d}$ (P_d is as defined in (11)), and θ are the amplitude and phase of the direct signal, respectively. The second term in (12) is the contribution of the diffuse component which is the sum of signals scattered from the tree components. $N = 7$ is the total number of scattering tree components (the trunk, branches, and subbranches; see Figure 7). $a_f = \sqrt{P_f/N}$ is the amplitude of each scattered signal (assumed to be equal for all scattered components), where P_f is as defined in (11), θ_i is the phase uniformly distributed within the range $[0, 2\pi]$, λ is the wavelength, and $\Delta L_i(t)$ is the time varying path length difference due to displacement of the ith tree component shown in Figure 7. Note from (12) that the time varying path length difference, $\Delta L_i(t)$, results in time varying phase changes which in turn gives a fading effect to the received signal. Following the same approach as in (6), $\Delta L_i(t)$ for $i = 1, 2, \ldots, 6$ are given by

$$\begin{aligned}
\Delta L_0(t) &\approx x_0(t)\frac{d_0(L_1+L_2)}{L_1L_2},\\
\Delta L_1(t) &\approx \big(x_0(t)+x_1(t)\big)\frac{d_1(L_1+L_2)}{L_1L_2},\\
\Delta L_2(t) &\approx \big(x_0(t)+x_1(t)+x_2(t)\big)\frac{d_2(L_1+L_2)}{L_1L_2},\\
\Delta L_3(t) &\approx \big(x_0(t)+x_3(t)\big)\frac{d_3(L_1+L_2)}{L_1L_2},\\
\Delta L_4(t) &\approx \big(x_0(t)+x_3(t)+x_4(t)\big)\frac{d_4(L_1+L_2)}{L_1L_2},\\
\Delta L_5(t) &\approx \big(x_0(t)+x_5(t)\big)\frac{d_5(L_1+L_2)}{L_1L_2},\\
\Delta L_6(t) &\approx \big(x_0(t)+x_5(t)+x_6(t)\big)\frac{d_6(L_1+L_2)}{L_1L_2},
\end{aligned} \tag{13}$$

where L_1, L_2, and d_i are as defined in (6), and $x_i(t)$ is obtained from the state-space model in (9) and (10).

Examples of simulated signal fading due to swaying tree using the new model for low- and high-wind speed conditions are shown in Figures 9 and 10, respectively. The simulation parameters are given in Table 3. In general, A_i values in the range 10 to 80 m^2, m_i values in the range 0.01 to 30 kg, k_i values in the range 5×10^2 to 5×10^4 N/m^2, c_i values in the range 0 to 35 can be used in the model. These parameter ranges are obtained by performing simulations using different tree parameters and comparing the simulated first and second-order statistics to these of measurements from Site 1 (since the new model is intended for modeling signal fading due to a single tree). Then, the parameter ranges are defined based on the agreements found between the measured and simulated first- and second-order statistics. Finally, realistic values within the defined parameter ranges are assigned to each tree component; see Table 3 (no curve fitting or numerical optimization is used). For example, as shown above the parameter range found for m_i is between 0.01 to 30 kg, from this a realistic value for m_0 (the trunk) should be close to the upper limit of the parameter rage,that is, somewhere between 15 to 30 kg. In this case, 20 kg is randomly chosen from the realistic value range for m_0; see Table 3. The same selection process based on realistic values within parameter ranges is performed for the other tree parameters. Comparisons of the cumulative distribution functions (CDFs), autocorrelation functions (ACFs), level-crossing rates (LCRs), and average fade durations (AFDs) of the measured and simulated received signals at different frequencies are shown in Figures 11–18. The LCRs and AFDs are normalized to the Root-Mean-Square (RMS) level. The CDF describes the probability distribution of a random variable. While the ACF is a measure of the degree to which two time samples of the same random process are related and is expressed as [21]

$$R_h(t_1, t_2) = E\{h(t_1)h(t_2)\}, \tag{14}$$

where E is the expectation, $h(t_1)$ and $h(t_2)$ are random variables obtained by observing $h(t)$ at time t_1 and t_2, respectively. The LCR measures the rapidity of the signal fading. It determines how often the fading crosses a given threshold in the positive-going direction [22]. The AFD quantifies how long the signal spends below a given threshold, that is, the average time between negative and positive level-crossings [22]. The CDF, ACF, LCR, and AFD determine the first- and second-order statistics of the channel.

The effect of wind speed on the channel statistics can be observed from Figures 11–14 which show comparisons of measured (leaved dry deciduous trees (Site 1) at 29 GHz) and simulated channel statistics during low- and high-wind speed conditions. We can observe from Figure 11 that the probability the received signal is less than a given threshold increases with increasing wind speed. Note also from Figure 12 how fast the ACF decays during high wind speed compared to low wind speed conditions. The increase

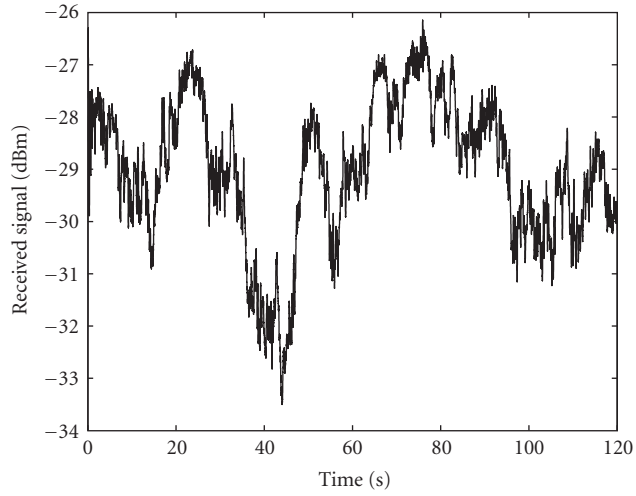

Figure 9: Simulated signal fading using the new model at 29 GHz during low wind speed conditions ($w_m = 2$ m/s). All simulation parameters are given in Table 3.

rate of signal changing activity during windy conditions can be implied from the LCR curves in Figure 13. In addition, the effect of high wind speed which results in deep signal fading with short durations can be observed from the AFD curves shown in Figure 14. The frequency dependency of the channel is evident from Figure 15–18 which show comparisons between measured (leaved dry deciduous trees (Site 1) at 2.45, 5.25, and 60 GHz) and simulated channel statistics during high wind speed conditions ($w_m = 5$ m/s). The probability that the received signal is less than a given threshold increases with increasing frequency; see Figure 15. We can also observe from Figure 16 that the autocorrelation function decays more rapidly for high frequency compared to low-frequency signals. The increasing rate of signal changing activity and the increasing existence of deep signal fading with increasing frequency can be observed from the LCR and AFD curves shown in Figures 17 and 18, respectively. The frequency dependency of the channel statistics is directly related to the signal wavelength. As the frequency increases, the signal wavelength decreases which results in increasing sensitivity to path length differences caused by swaying tree components. In general, the agreements found between the measured and simulated received signals in terms of both first- and second-order statistics are satisfactory; see Figures 11–18. Moreover, the results shown in Figures 11–18 suggest that the swaying of tree components with wind can highly impact the quality and availability of a given link, and should be considered when designing and evaluating systems at different frequencies.

5. Conclusion

In this paper, we use available measurements at 2.45, 5.25, 29, and 60 GHz, and wind speed data to study the dynamic

Table 3: Simulation parameters.

Wind parameters		Other parameters
$w_m = 2$ m/s (low wind)	$C_d = 0.35$ [16]	K-factor for 2.45 GHz = 6 dB (at $w_m = 5$ m/s)
$w_m = 5$ m/s (high wind)	$\rho = 1.226$ kg/m^3 [16]	K-factor for 5.25 GHz = 1 dB (at $w_m = 5$ m/s)
$k_\sigma = 0.434$	$T_s = 0.002$ s	K-factor for 29 GHz = 11 dB (at $w_m = 2$ m/s)
$h = 10$ m		K-factor for 29 GHz = -5 dB (at $w_m = 5$ m/s)
		K-factor for 60 GHz = -6 dB (at $w_m = 5$ m/s)
		$L_1 = 3000$ m and $L_2 = 100$ m

Tree parameters				
$d_0 = 1.0$ m	$A_0 = 66.2$ m^2	$m_0 = 20$ kg	$k_0 = 1.0 \times 10^4$ N/m	$c_0 = 20.0$
$d_1 = 3.0$ m	$A_1 = 21.0$ m^2	$m_1 = 1.0$ kg	$k_1 = 1.0 \times 10^3$ N/m	$c_1 = 15.0$
$d_2 = 3.7$ m	$A_2 = 7.80$ m^2	$m_2 = 0.02$ kg	$k_2 = 7.0 \times 10^3$ N/m	$c_2 = 2.00$
$d_3 = 2.5$ m	$A_3 = 22.9$ m^2	$m_3 = 2.0$ kg	$k_3 = 6.0 \times 10^2$ N/m	$c_3 = 14.0$
$d_4 = 2.7$ m	$A_4 = 9.70$ m^2	$m_4 = 0.03$ kg	$k_4 = 8.0 \times 10^3$ N/m	$c_4 = 1.80$
$d_5 = 2.8$ m	$A_5 = 23.5$ m^2	$m_5 = 2.5$ kg	$k_5 = 1.1 \times 10^3$ N/m	$c_5 = 14.5$
$d_6 = 3.2$ m	$A_6 = 10.4$ m^2	$m_6 = 0.04$ kg	$k_6 = 5.0 \times 10^3$ N/m	$c_6 = 2.00$

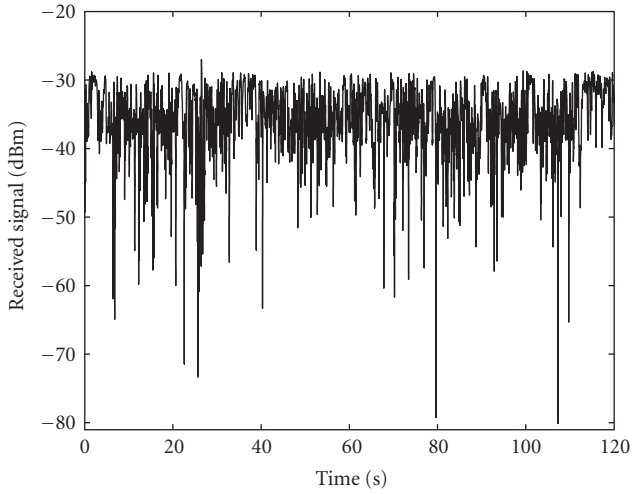

Figure 10: Simulated signal fading using the new model at 29 GHz during high wind speed conditions ($w_m = 5$ m/s). All simulation parameters are given in Table 3.

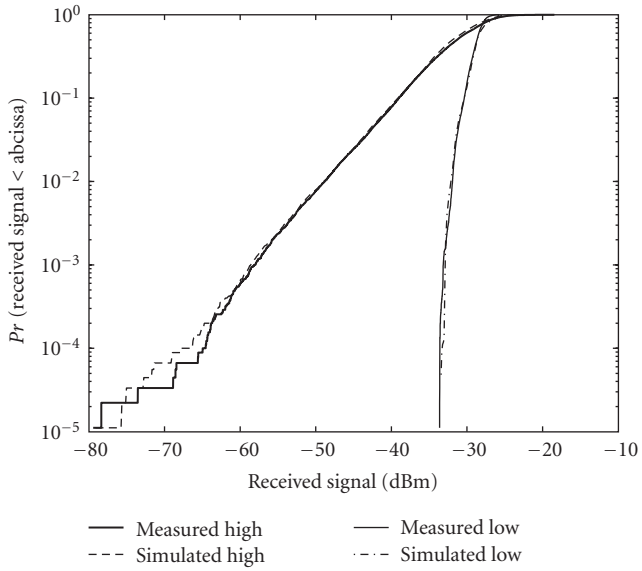

Figure 11: CDFs of measured (dry leaved deciduous trees (Site 1)) and simulated (using the new model) signals at 29 GHz during low ($w_m = 2$ m/s) and high ($w_m = 5$ m/s) wind speed conditions. All simulation parameters are given in Table 3.

effects of vegetation on propagating radiowaves. A new simulation model for generating signal fading due to a swaying tree has been developed by utilizing a multiple mass-spring system to represent a tree and a turbulent wind model. The model is validated in terms of first- and second-order statistics such as CDF, ACF, LCR, and AFD using measurements. The agreements found between the measured and simulated first- and second-order statistics of the received signals through vegetation are satisfactory. Furthermore, Ricean K-factors for different wind speeds are estimated from measurements. In general, the new model has similar dynamical and statistical characteristics as those observed from measurement results and can be used for simulating different capacity enhancing techniques such as adaptive coding and modulation and other fade mitigation techniques.

Appendices

A. Path Length Difference due to Swaying Tree Component

Using a trigonometric analysis of the paths shown in Figure 6, L_3 and L_4 can be expressed as

$$L_3 = \sqrt{L_1^2 + d^2} = L_1\sqrt{1 + \frac{d^2}{L_1^2}},$$
$$L_4 = \sqrt{L_2^2 + d^2} = L_2\sqrt{1 + \frac{d^2}{L_2^2}}. \quad \text{(A.1)}$$

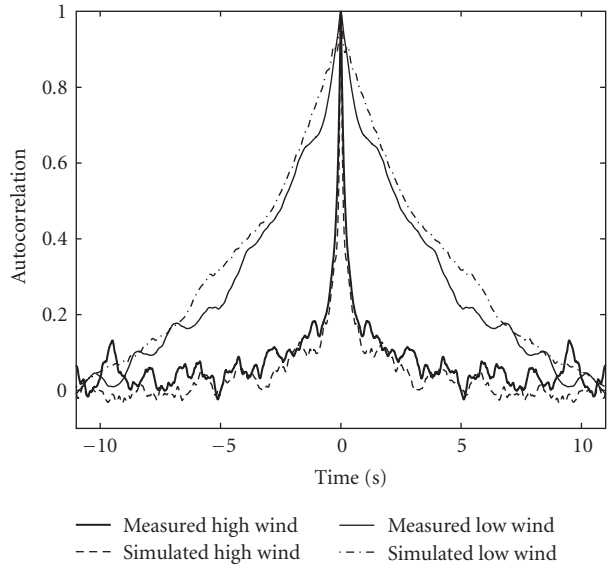

Figure 12: ACFs of measured (dry leaved deciduous trees (Site 1)) and simulated (using the new model) signals at 29 GHz during low ($w_m = 2$ m/s) and high ($w_m = 5$ m/s) wind speed conditions. All simulation parameters are given in Table 3.

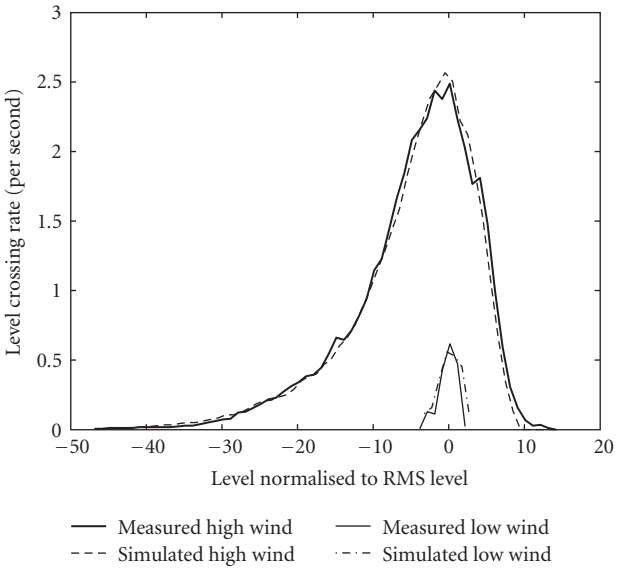

Figure 13: LCRs of measured (dry leaved deciduous trees (Site 1)) and simulated (using the new model) signals at 29 GHz during low ($w_m = 2$ m/s) and high ($w_m = 5$ m/s) wind speed conditions. All simulation parameters are given in Table 3.

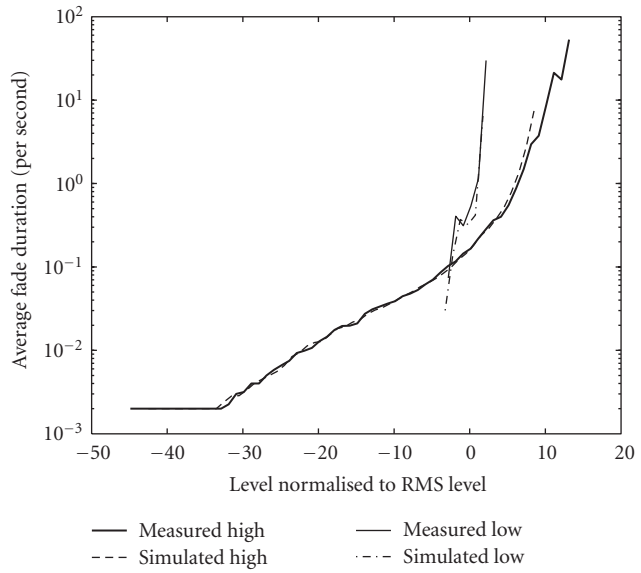

Figure 14: AFDs of measured (dry leaved deciduous trees (Site 1)) and simulated (using the new model) signals at 29 GHz during low ($w_m = 2$ m/s) and high ($w_m = 5$ m/s) wind speed conditions. All simulation parameters are given in Table 3.

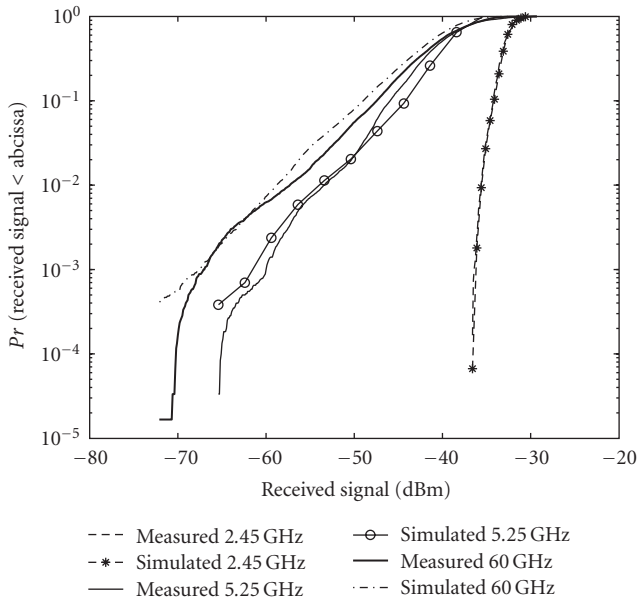

Figure 15: CDFs of measured (dry leaved deciduous trees (Site 1)) and simulated (using the new model) signals at 2.45, 5.25, and 60 GHz during high ($w_m = 5$ m/s) wind speed conditions. All simulation parameters are given in Table 3.

Assuming $L_1 \gg d$ and $L_2 \gg d$, Taylor approximation can be applied to yield

$$L_3 \approx L_1\left(1 + \frac{d^2}{2L_1^2}\right),$$
$$L_4 \approx L_2\left(1 + \frac{d^2}{2L_2^2}\right). \tag{A.2}$$

$L_3 + L_4$ is the path length when a tree component is at rest, and by using (A.2), we get

$$L_3 + L_4 \approx L_1 + L_2 + \frac{d^2}{2}\left(\frac{L_1 + L_2}{L_1 L_2}\right). \tag{A.3}$$

$L_5 + L_6$ is the path length when a tree component is displaced. Again performing a trigonometric analysis of Figure 6 and

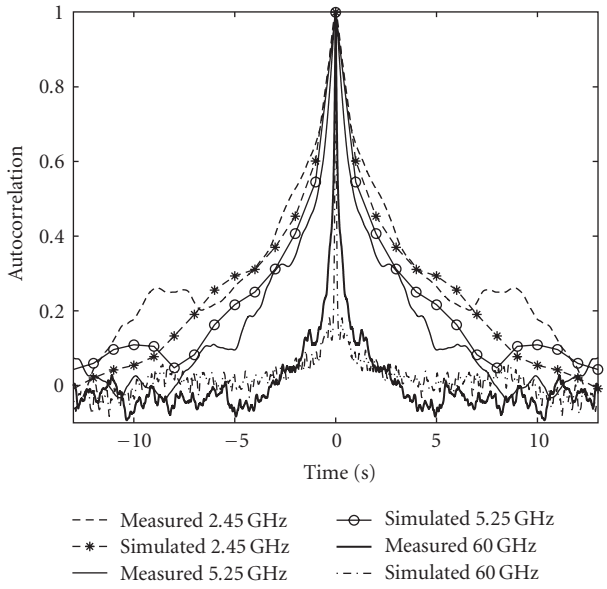

Figure 16: ACFs of measured (dry leaved deciduous trees (Site 1)) and simulated (using the new model) signals at 2.45, 5.25, and 60 GHz during high ($w_m = 5$ m/s) wind speed conditions. All simulation parameters are given in Table 3.

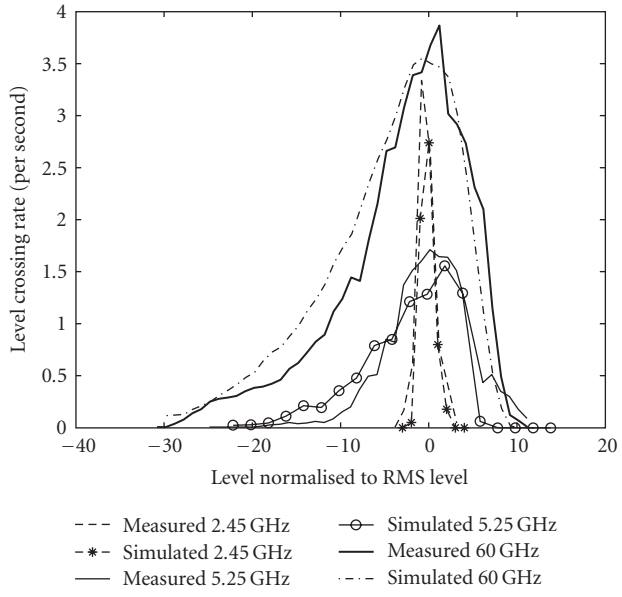

Figure 17: LCRs of measured (dry leaved deciduous trees (Site 1)) and simulated (using the new model) signals at 2.45, 5.25, and 60 GHz during high ($w_m = 5$ m/s) wind speed conditions. All simulation parameters are given in Table 3.

applying a Taylor approximation by assuming $L_1 \gg d + x$ and $L_2 \gg d + x$, $L_5 + L_6$ can be expressed as

$$L_5 + L_6 \approx L_1 + L_2 + \frac{(d+x)^2}{2}\left(\frac{L_1 + L_2}{L_1 L_2}\right). \tag{A.4}$$

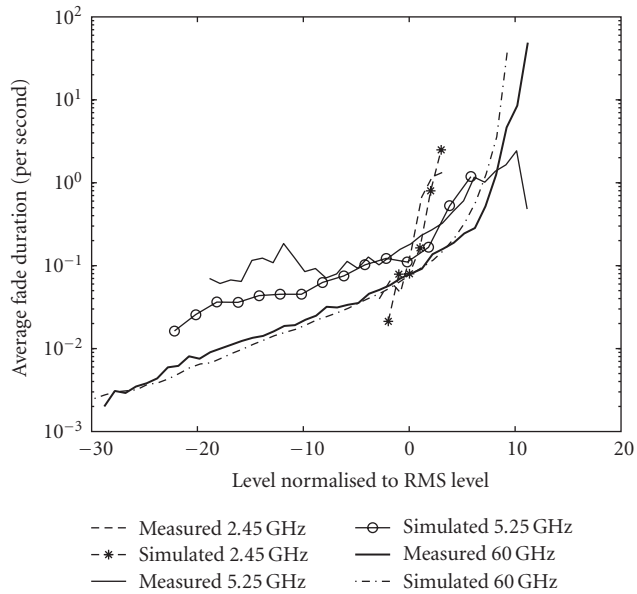

Figure 18: AFDs of measured (dry leaved deciduous trees (Site 1)) and simulated (using the new model) signals at 2.45, 5.25, and 60 GHz during high ($w_m = 5$ m/s) wind speed conditions. All simulation parameters are given in Table 3.

The difference in path length when a tree component is at rest and when it is displaced is then given by

$$\begin{aligned}\Delta L &= (L_5 + L_6) - (L_3 + L_4) \\ &\approx \left(\frac{2dx + x^2}{2}\right)\left(\frac{L_1 + L_2}{L_1 L_2}\right).\end{aligned} \tag{A.5}$$

Assuming further $x \ll d$ (which is valid for trees not located very near the transmitter or the receiver), the path length difference can then be expressed as

$$\Delta L \approx xd\left(\frac{L_1 + L_2}{L_1 L_2}\right). \tag{A.6}$$

B. Matrices for the State-Space Model

The state, $\mathbf{y}$, and input, $\mathbf{u}$, vectors defined in (9) and (10) are given by

$$\mathbf{y} = \left[x_0(t) \;\; \cdots \;\; x_6(t) \;\; \dot{x}_0(t) \;\; \cdots \;\; \dot{x}_6(t)\right]^T, \tag{B.1}$$

$$\mathbf{u} = \left[f_0(t) \;\; \cdots \;\; f_6(t)\right]^T. \tag{B.2}$$

By taking the first derivation of (B.1),

$$\dot{\mathbf{y}} = \left[\dot{x}_0(t) \;\; \cdots \;\; \dot{x}_6(t) \;\; \ddot{x}_0(t) \;\; \cdots \;\; \ddot{x}_6(t)\right]^T, \tag{B.3}$$

where the double derivations $\ddot{x}_0(t) \cdots \ddot{x}_6(t)$ in (B.3) are defined in (7). From (9), $\dot{\mathbf{y}}$ is given by

$$\dot{\mathbf{y}} = \mathbf{A}\mathbf{y} + \mathbf{B}\mathbf{u}, \tag{B.4}$$

where $\mathbf{y}$ and $\mathbf{u}$ are as defined in (B.1) and (B.2). In order (B.4) to be equal to (B.3), the matrices $\mathbf{A}$ and $\mathbf{B}$ have to be equal to

$$\mathbf{A} = \begin{pmatrix} \mathbf{0}_{7\times7} & \mathbf{I}_{7\times7} \\ \mathbf{A_{21}} & \mathbf{A_{22}} \end{pmatrix}, \tag{B.5}$$

where $\mathbf{0}_{7\times7}$ and $\mathbf{I}_{7\times7}$ are 7×7 zero and identity matrices, respectively. $\mathbf{A_{21}}$ and $\mathbf{A_{22}}$ in (B.5) are given by

$$\mathbf{A_{21}} = \begin{pmatrix} -\frac{(k_0+k_1+k_3+k_5)}{m_0} & \frac{k_1}{m_0} & 0 & \frac{k_3}{m_0} & 0 & \frac{k_5}{m_0} & 0 \\ \frac{k_1}{m_1} & -\frac{(k_1+k_2)}{m_1} & \frac{k_2}{m_1} & 0 & 0 & 0 & 0 \\ 0 & \frac{k_2}{m_2} & -\frac{k_2}{m_2} & 0 & 0 & 0 & 0 \\ \frac{k_3}{m_3} & 0 & 0 & -\frac{(k_3+k_4)}{m_3} & \frac{k_4}{m_3} & 0 & 0 \\ 0 & 0 & 0 & \frac{k_4}{m_4} & -\frac{k_4}{m_4} & 0 & 0 \\ \frac{k_5}{m_5} & 0 & 0 & 0 & 0 & -\frac{(k_5+k_6)}{m_5} & \frac{k_6}{m_5} \\ 0 & 0 & 0 & 0 & 0 & \frac{k_6}{m_6} & -\frac{k_6}{m_6} \end{pmatrix}, \tag{B.6}$$

$$\mathbf{A_{22}} = \begin{pmatrix} -\frac{(c_0+c_1+c_3+c_5)}{m_0} & \frac{c_1}{m_0} & 0 & \frac{c_3}{m_0} & 0 & \frac{c_5}{m_0} & 0 \\ \frac{c_1}{m_1} & -\frac{(c_1+c_2)}{m_1} & \frac{c_2}{m_1} & 0 & 0 & 0 & 0 \\ 0 & \frac{c_2}{m_2} & -\frac{c_2}{m_2} & 0 & 0 & 0 & 0 \\ \frac{c_3}{m_3} & 0 & 0 & -\frac{(c_3+c_4)}{m_3} & \frac{c_4}{m_3} & 0 & 0 \\ 0 & 0 & 0 & \frac{c_4}{m_4} & -\frac{c_4}{m_4} & 0 & 0 \\ \frac{c_5}{m_5} & 0 & 0 & 0 & 0 & -\frac{(c_5+c_6)}{m_5} & \frac{c_6}{m_5} \\ 0 & 0 & 0 & 0 & 0 & \frac{c_6}{m_6} & -\frac{c_6}{m_6} \end{pmatrix}, \tag{B.7}$$

$$\mathbf{B} = \begin{pmatrix} \mathbf{0}_{7\times7} \\ \mathbf{B_{21}} \end{pmatrix}, \tag{B.8}$$

where $\mathbf{B_{21}}$ in (B.8) is a diagonal matrix expressed as $\mathbf{B_{21}} = \text{diag}\{1/m_0 \cdots 1/m_6\}$.

The output vector $\mathbf{x}$ in (10) is defined as

$$\mathbf{x} = \begin{bmatrix} x_0(t) & \cdots & x_6(t) \end{bmatrix}^T. \tag{B.9}$$

From (10), $\mathbf{x}$ is given by

$$\mathbf{x} = \mathbf{C}\mathbf{y} + \mathbf{D}\mathbf{u}. \tag{B.10}$$

For (B.10) to be equal to (B.9), the matrices $\mathbf{C}$ and $\mathbf{D}$ have to be equal to

$$\begin{aligned} \mathbf{C} &= (\mathbf{I}_{7\times7} \quad \mathbf{0}_{7\times7}), \\ \mathbf{D} &= (\mathbf{0}_{7\times7}). \end{aligned} \tag{B.11}$$

Acknowledgments

This work is supported by the research council of Norway (NFR). The authors would like to thank the Communications Research Centre Canada (CRC), especially Simon Perras for providing measurement data. The authors would like also to thank Morten Topland of UNIK for fruitful discussions.

References

[1] M. Cheffena, *Modeling and prediction of millimeter wavelength channels*, Ph.D. thesis, Norwegian University of Science and Technology, Trondheim, Norway, October 2008.

[2] M. O. Al-Nuaimi and A. M. Hammoudeh, "Measurements and predictions of attenuation and scatter of microwave signals by trees," *IEE Proceedings: Microwaves, Antennas and Propagation*, vol. 141, no. 2, pp. 70–76, 1994.

[3] I. J. Dilworth and B. L'Ebraly, "Propagation effects due to foliage and building scatter at millimetre wavelengths," in *Proceedings of the 9th International Conference on Antennas and Propagation*, vol. 2, pp. 51–53, Eindhoven, The Netherlands, April 1995.

[4] Recommendation ITU-R P.833-5, "Attenuation in vegetation," Tech. Rep. P.833-2, ITU, Geneva, Switzerland, 2005.

[5] A. M. Randle, *Dynamic radio channel effects from L-band foliage scatter*, Ph.D. thesis, University of York, York, UK, September 1999.

[6] K. H. Craig, Ed., "Propagation planning procedures for LMDS," AC215 CRABS, Deliverable D3P1b, January 1999, http://www.telenor.no/fou/prosjekter/crabs.

[7] S. Perras and L. Bouchard, "Fading characteristics of RF signals due to foliage in frequency bands from 2 to 60 GHz," in *Proceedings of the 5th International Symposium on Wireless Personal Multimedia Communications*, vol. 1, pp. 267–271, Honolulu, Hawaii, USA, October 2002.

[8] M. H. Hashim and S. Stavrou, "Dynamic impact characterization of vegetation movements on radiowave propagation in controlled environment," *IEEE Antennas and Wireless Propagation Letters*, vol. 2, no. 1, pp. 316–318, 2003.

[9] T. Sofos and P. Constantinou, "Propagation model for vegetation effects in terrestrial and satellite mobile systems," *IEEE Transactions on Antennas and Propagation*, vol. 52, no. 7, pp. 1917–1920, 2004.

[10] M. Cheffena and T. Ekman, "Modeling the dynamic effects of vegetation on radiowave propagation," in *Proceedings of the IEEE International Conference on Communications (ICC '08)*, pp. 4466–4471, Beijing, China, May 2008.

[11] W. E. Leithead, S. de la Salle, and D. Reardon, "Role and objectives of control for wind turbines," *IEE Proceedings C*, vol. 138, no. 2, pp. 135–148, 1991.

[12] C. Nichita, D. Luca, B. Dakyo, and E. Ceanga, "Large band simulation of the wind speed for real time wind turbine simulators," *IEEE Transactions on Energy Conversion*, vol. 17, no. 4, pp. 523–529, 2002.

[13] E. B. Muhando, T. Senjyu, N. Urasaki, A. Yona, H. Kinjo, and T. Funabashi, "Gain scheduling control of variable speed WTG under widely varying turbulence loading," *Renewable Energy*, vol. 32, no. 14, pp. 2407–2423, 2007.

[14] "*European Standard for Wind Loads*," Eurocode EN 1991-1-4, WIND ACTION.

[15] K. R. James, N. Haritos, and P. K. Ades, "Mechanical stability of trees under dynamic loads," *American Journal of Botany*, vol. 93, no. 10, pp. 1522–1530, 2006.

[16] H. Peltola, S. Kellomäki, H. Väisänen, and V.-P. Ikonen, "A mechanistic model for assessing the risk of wind and snow damage to single trees and stands of Scots pine, Norway spruce, and birch," *Canadian Journal of Forest Research*, vol. 29, no. 6, pp. 647–661, 1999.

[17] J. C. DalBello, G. L. Siqueira, and H. L. Bertoni, "Effects of vegetation on urban cellular systems," in *Proceedings of IEEE International Conference on Universal Personal Communications (ICUPC '98)*, vol. 1, pp. 113–116, Florence, Italy, October 1998.

[18] A. Kajiwara, "LMDS radio channel obstructed by foliage," in *Proceedings of IEEE International Conference on Communications (ICC '00)*, vol. 3, pp. 1583–1587, New Orleans, La, USA, June 2000.

[19] N. Naz and D. D. Falconer, "Temporal variations characterization for fixed wireless at 29.5 GHz," in *Proceedings of the 51st IEEE Vehicular Technology Conference (VTC '00)*, vol. 3, pp. 2178–2182, Tokyo, Japan, May 2000.

[20] L. J. Greenstein, D. G. Michelson, and V. Erceg, "Moment-method estimation of the Ricean K-factor," *IEEE Communications Letters*, vol. 3, no. 6, pp. 175–176, 1999.

[21] B. Sklar, *Digital Communications*, Prentice-Hall, Englewood Cliffs, NJ, USA, 2001.

[22] S. R. Saunders, *Antennas and Propagation for Wireless Communication Systems*, John Wiley & Sons, New York, NY, USA, 2003.